ChemPubSoc Europe

DOI: 10.1002/open.201900076

Open Access ChemistryOPEN Full Papers

Special Collection

Steric and Electronic Effects in Gold N-Heterocyclic Carbene Complexes Revealed by Computational Analysis

Sunel de Kock, Jan Dillen, and Catharine Esterhuysen*[a]

A computational analysis of a series of cationic and neutral gold imidazolylidene and benzimidizolylidene complexes is reported. The Bond Dissociation Energies of the various ligands in the complexes calculated at the PBE0-D3/def2-TZVP level of theory increase with increasing ligand volume, except for those of complexes containing t-butyl-substituted ligands, which are anomalously low particularly for the benzimidazolylidene species. Atoms in Molecules studies show the presence of a variety of weak intramolecular interactions, characterised by the presence of bond critical points with a range of different properties. Energy Decomposition Analysis and calculation of Electrostatic Surface Potentials indicate that some interactions are weakly attractive dispersion-type interactions, while others are repulsive. The octanol/water partition coefficients (log P values) were calculated as a measure of the lipophilicities of the complexes and were found to increase with increasing volume.

1. Introduction

Since the discovery of the first stable crystalline N-heterocyclic carbene (NHC) in 1991,[1] this ligand class has gone from relative obscurity to enjoying widespread use in many areas of transition metal chemistry, most notably homogeneous catalysis.[2] Initial interest in NHCs stemmed from their similarity to the well-established phosphine ligands, but NHCs have long since distinguished themselves and are now recognised to possess a rich chemistry of their own.[3] Like phosphines, NHCs are strong σ donors, but surpass even trialkyl phosphines in terms of their electron-donating ability.[4] Besides the enhanced stability they confer to metal complexes, NHCs also have the advantage over phosphine ligands in the ease with which libraries of structurally related NHC ligands may be synthesized.[2] The outstanding properties of NHCs have led to them becoming ubiquitous ligands in the field of organometallic catalysis,[5,6] and stimulated research into the medicinal properties of NHC metal complexes.[7,8]

Similarly to phosphine and cyclopentadienyl ligands, much of the popularity of NHCs originates from their electronic and steric tunability, which can to some extent be varied independently.[3] Changing the nature of the heterocycle and the substituents at the back of the ring are the most common strategies employed in modifying the NHC electronic properties,[9] but in some cases this has been found to also affect the steric properties of the ligand, which can result in a weakening of the metal-NHC bond.[10–12] In NHCs with aryl groups at the N-substituents, electron-donating or -withdrawing groups at the *para* position can also be used to tune the electronic properties,[13] but in general, little effect of the N-substituents on the electronic properties is observed.[14] Nevertheless, varying the size of alkyl N-substituents has also emerged as a successful strategy in generating NHC complexes of differing lipophilicity, an important parameter influencing drug uptake.[15,16]

The cationic lipophilic character of a range of Au(I) complexes with the 1,3-diethylbenzylimidazol-2-ylidene ligand[17–19] has been shown to be important for inducing anti-mitochondrial effects, while the stability of the coordination bonds, *i.e.* strength of the Au-ligand bond (as estimated with bond dissociation energies, BDEs, calculated by density functional theory) is predictive of the affinity of the complexes for the TrxR enzyme.[17] TrxR is an abundant selenoprotein that is the only known enzyme to reduce thioredoxin (Trx);[20] a lower BDE could thus be associated with stronger TrxR inhibition and yield a greater effect on tumour progression and development,[21] but also with unwanted binding to serum albumin.[17]

Lipophilicity has also been shown to correlate with the anti-mitochondrial activity of a series of cationic, linear Au(I) NHCs (compounds $N2^+$, $N4^+$, $N5^+$ and $N6^+$ in Scheme 1),[16] but the related benzylimidazol-2-ylidene ligands (compound denoted by Nxb^+ in Scheme 1) were not studied in this context. To gain greater insight into the subtle interplay of electronic and steric effects operating in these NHC coordination complexes, we computationally investigated the effect of varying the alkyl moiety attached at the N-substituent position, and the type of NHC ligand (imidazolylidene versus less electron-donating benzimidazolylidene), on the metal ligand bond, and hence on the BDEs.

The different NHC ligands studied are shown in Scheme 1, in order of increasing volume and hence increasing lipophilicity. By investigating both the cationic homo-ligated Au-NHC

[a] S. de Kock, Prof. Dr. J. Dillen, Prof. Dr. C. Esterhuysen
Department of Chemistry and Polymer Science
Stellenbosch University
Private Bag X1, Matieland, Stellenbosch, 7602, South Africa
E-mail: ce@sun.ac.za

Supporting information for this article is available on the WWW under https://doi.org/10.1002/open.201900076

An invited contribution to a Special Collection dedicated to Computatonal Chemistry

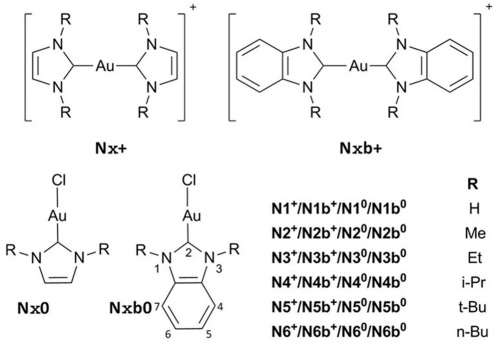

Scheme 1. Cationic and neutral Au(I) complexes investigated in this study, numbered according to increasing molecular volume.

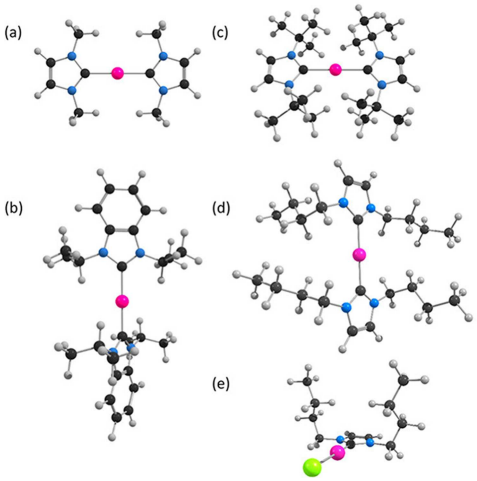

Figure 1. Minimum energy conformations of (a) N1+, (b) N4b+, (c) N5+, (d) $N6^+$ and (e) $N6^0$. (Pink = Au, blue = N, green = Cl, black = C, light grey = H.)

complexes (indicated by a '+' in the compound code) as well as the neutral complexes (identified by '0') with one NHC and one Cl ligand we aimed to compare the BDEs to identify which complexes could be more efficient prodrugs. In addition, an Atoms in Molecules analysis indicated the presence of numerous intramolecular interactions between the NHC ligands with the metal, and with each other. These interactions may also play a significant role in the mechanism of action of these complexes as prodrugs, hence we investigated them further by undertaking an Energy Decomposition Analysis and calculating the electrostatic surface potentials (ESPs).

2. Results and Discussion

2.1. Complex Structures

The geometries of the Au complexes shown in Scheme 1, as well as their mono-ligated variants and individual NHC ligands, were optimised at the PBE0-D3/TZVP level of theory (coordinates included in ESI). Selected structures are given in Figure 1, while selected geometric parameters for cationic and neutral complexes, along with the available crystal structure parameters are shown in Tables 1 and 2, respectively (the Cambridge Structural Database,[22] CSD, refcodes are indicated for reference).

In order to validate our model chemistry we compared the Au complex structures derived from the geometry optimisations to those observed in the crystal structures of these complexes. The conformational flexibility of the N-substituent alkyl chains and the weakness of the interactions between them result in many stationary points on a rather flat potential energy surface; however, the optimised geometries of the lowest energy

Table 1. Selected geometrical parameters from optimised geometries of cationic complexes, with relevant crystal structure parameters for comparison.

	Optimised geometry			CSD refcode	Crystal structure		
	Au–C (Å)	C–Au-C (°)	N–C–C–N (°)		Au–C (Å)	C–Au–C (°)	N–C–C–N (°)
$N1^+$	2.03	180.0	90.0	UMAGUL[23]	2.02, 2.02, 2.01, 2.02	176.7, 178.3	160.7, 168.8, 176.2, 163.2
$N1b^+$	2.03	180.0	90.0				
$N2^+$	2.04	180.0	90.0	KIZVOG[24]	2.03, 2.03	178.4	176.4, 177.8
				KIZVUM[24]	2.03	180.0	180.0
				ORUHUF[25]	2.02, 2.01	177.4	176.5, 175.4
				YERFAD[16]	2.02	180.0	180.0
$N2b^+$	2.04	180.0	90.0	FIBXUK[26]	2.05	180.0	180.0
				KIZWAT[24]	2.02	180.0	180.0
				KIZWEX[24]	2.10	180.0	180.0
				XIRMUI[27]	2.01	180.0	180.0
$N3^+$	2.03	180.0	125.8				
$N3b^+$	2.03	180.0	119.5	FIBYAR[26]	2.02, 2.02	175.0	129.9, 129.1
				FIBYEV[26]	2.00	180.0	180.0
$N4^+$	2.04	180.0	90.0	YERFIL[16]	2.03	180.0	180.0
$N4b^+$	2.04	180.0	126.7	CIVMIE[28]	2.02, 2.03	175.6	147.5, 165.6
				XIQKOZ[29]	2.02	180.0	118.0
$N5^+$	2.06	180.0	126.5	NEYQAL[30]	2.05, 2.05	176.9	115.1, 105.4
				YERFUX[16]	2.03, 2.04	176.1	101.1, 94.2
$N5b^+$	2.06	172.3	72.8, 126.2				
$N6^+$	2.03	180.0	180.0	YERFOR[16]	2.03, 2.03, 2.05, 2.05, 2.04, 2.01	180.0, 180.0, 178.3	180.0, 180.0, 180.0, 180.0, 177.9, 172.9
$N6b^+$	2.03	180.0	180.0				

Table 2. Selected geometrical parameters from optimised geometries of neutral complexes, with relevant crystal structure parameters for comparison.

	Optimised geometry			CSD refcode	Crystal structure		
	Au–C (Å)	Au–Cl (Å)	C–Au–Cl (°)		Au–C (Å)	Au–Cl (Å)	C–Au–Cl (°)
$N1^0$	1.98	2.26	180.0				
$N1b^0$	1.97	2.26	180.0				
$N2^0$	1.99	2.27	180.0	ECIHOO[15]	1.95, 1.93, 1.94	2.30, 2.28, 2.27	178.9, 178.3, 179.2
				FIBXIY[26]	1.98	2.29	178.8
$N2b^0$	1.98	2.26	180.0				
$N3^0$	1.99	2.27	180.0				
$N3b^0$	1.98	2.27	180.0	KEKQIA[31]	2.00	2.30	179.8
$N4^0$	1.99	2.27	180.0	ECIHUU[15]	1.96	2.26	175.0
				ECIHUU01[32]	1.99	2.31	175.2
$N4b^0$	1.99	2.27	180.0	YIKXEW[33]	1.97	2.27	178.1
				YIKXEW01[28]	1.97	2.30	179.8
$N5^0$	2.01	2.27	180.0	FAWYIM[15]	2.02	2.27	180.0
$N5b^0$	2.02	2.27	180.0				
$N6^0$	1.99	2.27	178.8				
$N6b^0$	1.98	2.27	179.9	VUPCIT[34]	1.98	2.30	179.1

structures are very similar to those found experimentally, which is especially encouraging in the case of the normal-butyl (n-Bu) substituted species (**N6**$^+$, **N6b**$^+$, **N6**^{0} and **N6b**^{0}). This suggests that our choice of the PBE0-D3/TZVP level of theory is justified. Generally good agreement of the calculated Au–C bond lengths with crystal structures was found, although bond lengths are marginally shorter in the crystal structures (as would be expected owing to atomic vibrations in the experimental structure) and differences are observed when different counter ions or solvent molecules are present in the crystal structures. For instance, the **N2b**$^+$ complex (N-substituent = Me) differs from the crystal structure of KIZWEX[24] that was used as the starting point for the geometry optimisation; however, seen in conjunction with the three other crystal structures that contain **N2b**$^+$ with different counterions the average value for the Au–C bond length is similar to that in the optimised geometry. We suspect that the variation in bond length is related to solvent or counterion effects. The Au–C bond lengths of the cationic imidazolylidene and benzimidazolylidene species are mostly equivalent, but differ in the case of the isopropyl (i-Pr) and tertiary butyl (t-Bu) complexes, **N4**$^+$, **N4b**$^+$, **N5**$^+$ and **N5b**$^+$. For these species the Au–C bond length is slightly elongated, this being more pronounced for the t-Bu species, **N5**$^+$ and **N5b**$^+$.

Conversely, in the neutral complexes the Au–C bond in the imidazolylidene species is slightly longer than in the benzimidazolylidene species, which might be attributed to differences in the dipole moments of the complexes featuring the different heterocycles. As in the cationic species, the neutral i-Pr and t-Bu complexes are exceptions: **N4**^{0} and **N4b**^{0} have almost identical Au–C bond lengths, and **N5**^{0} has a *shorter* Au–C bond length than **N5b**^{0}. The optimised geometries of both the cationic and neutral complexes bearing t-Bu N-substituents (**N5**$^+$, **N5b**$^+$, **N5**^{0} and **N5b**^{0}) consistently have the longest Au–C bond lengths, indicative of strain at the metal centre due to the sterically demanding t-Bu groups. This is also the case in the crystal structures of **N5**$^+$ and **N5**^{0}, but unfortunately no crystal structures of **N5b**$^+$ or **N5b**^{0} exist for comparison.

The C–Au-C bond angles in both the crystal structures and optimised geometries show little deviation from linearity, as is the norm for Au in the +1 oxidation state.[35] However, **N5b**$^+$ displays a C–Au-C bond angle of 172° in the lowest energy structure determined by our conformational sampling and optimisation procedure, a significant deviation from the usual linear conformation.

The optimised geometries typically have N–C···(Au)···C–N dihedral angles closer to orthogonal, while in the crystal structures the NHC rings are more likely to be coplanar. The coplanar arrangement appears to facilitate closer packing of the NHC rings in the solid phase, while the ligands have more freedom to orient themselves during geometry optimisation in the absence of the periodic system. Relaxed scans of the NHC-NHC dihedral angles were performed for all the cationic complexes, excluding the distorted **N5b**$^+$ (for which the C–Au–C line does not lie in the plane of the NHC ligands), to investigate the energetic barrier to rotation of the NHC rings (see examples in Figure S1 in the ESI). The highest energy conformations have dihedral angles of ~180°, where the N-substituents on opposing rings are forced into close proximity to each other. The rotational barriers are low, ranging from less than half a kcal mol^{-1} up to 4.8 kcal mol^{-1} for **N5**$^+$, which is in agreement with NMR results[16] and suggest that all these conformational states should be accessible at room temperature.

In terms of the orientation of the N-substituents we observe excellent agreement between the lowest energy conformations determined by geometry optimisation and those found in the crystal structures. In the i-Pr species (**N4**$^+$, **N4b**$^+$, **N4**^{0} and **N4b**^{0}) the CH hydrogen atoms are pointed toward the metal centre, while the CH_3 groups are oriented away. Three of the t-Bu complexes have two CH_3 groups per N-substituent oriented toward the Au, while **N5b**$^+$ has only one. In **N6**$^+$ and **N6b**$^+$ the n-Bu N-substituents on opposite sides of the metal centre are aligned, while in **N6**^{0} and **N6b**^{0} the n-Bu chains of the *same* NHC ring are in alignment (Figure 1 (d) and (e)). This organisation in the n-Bu substituted species is indicative of stabilising dispersion interactions between the alkyl chains.

2.2. Atoms in Molecules

The minimum energy conformations shown in Figure 1 suggest that there may be intramolecular contacts between some of the ligands, so to investigate this further we performed Atoms in Molecules (AIM) analysis (molecular graphs of selected complexes are shown in Figure 2). Within the framework of AIM, the presence of a bond path (BP, a line of maximal electron density connecting two nuclei) and an associated bond critical point (BCP, a point of minimum electron density along the BP) are sufficient evidence of a bonding interaction,[36] although this has been disputed.[37] Furthermore, H···H bonding between congested hydrogen atoms has been a controversial topic in the literature,[38–40] and has provoked a more general speculation on the interpretation of objects in the electron density topology.[41–76] Martín Pendás *et al.* describe BPs as being "privileged exchange channels" along which atoms coordinate the spin of their electrons to minimise Pauli repulsion.[42] Despite this, even though BPs indicate stabilising local interactions, their presence does not imply a lowering of the total energy of the system. The establishment of BPs between congested atoms may be accompanied by an increase in their self energies or a reduction in the stabilisation provided by other bonding interactions in a molecule.[42] It is this energy increase that is often interpreted as steric repulsion.

BPs and BCPs were identified between several Au···H and H···H pairs (between N-substituent atoms on opposite sides of the metal centre) in the molecular graphs, as well as C···H BPs in **N5b$^+$** and **N5b^0** (Figure 2). The electron densities at the BCPs along the intramolecular interaction paths are low (Table 3), while the values of the Laplacian are positive and the kinetic energy density is close to zero in all cases, as expected for closed-shell interactions.[44]

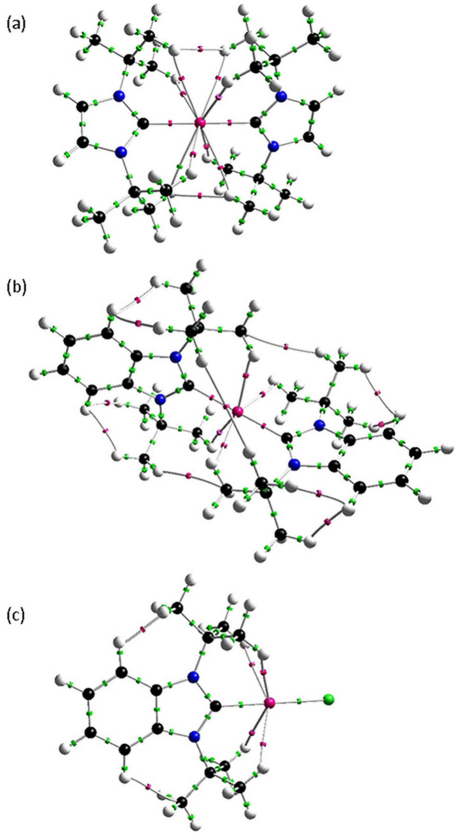

Figure 2. Molecular graphs of a) N5$^+$, b) N5b$^+$ and c) N5b^0. BCPs of weak, closed-shell interactions indicated in pink, covalent/coordination BCPs in green.

Table 3. Properties of BCPs of weak interactions. ρ is the electron density, $\nabla^2\rho$ is the Laplacian of the electron density, and K is the Hamiltonian kinetic energy at the BCP. Values in parenthesis indicate multiple instances of the interaction owing to molecular symmetry.

		Distance (Å)	ρ (*e* bohr^{-3})	∇^2 ρ (*e* bohr^{-5})	K (Ha bohr^{-3})
N3$^+$	H···H	2.99 (2)	0.002	0.007	−0.0005
N3b$^+$	H···H	3.29 (2)	0.001	0.004	−0.0003
N4b$^+$	C4-H···H	2.25 (4)	0.008	0.028	−0.0013
	C4-H···H	2.23 (4)	0.008	0.029	−0.0013
N4b^0	C4-H···H	2.24 (4)	0.008	0.028	−0.0013
	Au···H	2.62 (2)	0.017	0.054	−0.0013
N5$^+$	H···H	2.21 (2)	0.008	0.026	−0.0011
	Au···H	2.82 (4)	0.011	0.031	−0.0009
	Au···H	2.52 (4)	0.019	0.054	−0.0011
N5^0	Au···H	2.62 (4)	0.015	0.044	−0.0012
N5b$^+$	H···H	3.29	0.001	0.002	−0.0002
	H···C	3.23 (2)	0.002	0.009	−0.0006
	C4-H···H	2.10 (4)	0.011	0.037	−0.0015
	C4-H···H	1.97 (4)	0.015	0.051	−0.0019
	Au···H	2.48 (2)	0.022	0.070	−0.0009
	Au···H	2.47 (2)	0.023	0.072	−0.0009
N5b^0	C4-H···C	2.34 (2)	0.018	0.066	−0.0022
	Au···H	2.49 (4)	0.020	0.060	−0.0011
N6$^+$	H···H	2.87 (2)	0.003	0.011	−0.0008
	H···H	2.77 (2)	0.003	0.010	−0.0006
	H···H	2.49 (2)	0.004	0.013	−0.0006
	H···H	2.47 (2)	0.005	0.015	−0.0008
	Au···H	3.09 (2)	0.007	0.022	−0.0009
N6^0	H···H	2.60	0.003	0.009	−0.0004
	Au···H	3.23 (2)	0.006	0.017	−0.0006
N6b$^+$	H···H	2.81 (2)	0.003	0.009	−0.0006
	H···H	2.55 (2)	0.004	0.012	−0.0006
	H···H	2.44 (2)	0.005	0.016	−0.0007
	Au···H	3.10 (2)	0.007	0.022	−0.0006
N6b^0	H···H	2.62	0.003	0.008	−0.0004
	Au···H	3.22 (2)	0.006	0.017	−0.0007

The smallest complexes in which H···H interactions are observed are **N3$^+$** and **N3b$^+$**. The interatomic distances are substantially longer than twice the van der Waals radius of hydrogen[47] ($vdW_{H\cdots H}$ = 2.40 Å) and electron density at the BCPs is exceptionally low. Based on these factors, and the relative flexibility of the ethyl ligands, we interpret these BPs as weakly stabilising dispersion interactions between the alkyl chains. The H···H bonding interaction present in **N5b$^+$** appears even weaker, whereas **N5$^+$** (Figure 2) features a different conformation of its t-Bu N-substituents, which puts two pairs of hydrogen atoms in close proximity. The interatomic distance is shorter than $vdW_{H\cdots H}$ and a greater electron density is observed at the BCP. Given the rigidity of the t-Bu N-substituents and the short interatomic distance, this bonding interaction may have a slight

destabilising effect on the complex as a whole. The other H···H interactions between N-substituent hydrogen atoms occur in the n-Bu substituted species. **N6^0** and **N6b^0** feature one such interaction each, between the N-substituents on opposite sides of the NHC ring, while the cationic **N6$^+$** and **N6b$^+$** exhibit four and three such interactions, respectively, between the N-substituents on opposite sides of the metal centre. The n-Bu chains of the N-substituents in these species have a great deal more flexibility, based on the numerous other stationary points identified during sampling of the conformational space. In addition, the interatomic separations here are all close to $vdW_{H\cdots H}$. It therefore appears likely that these interactions have a stabilising effect on the complexes. It should be noted, however, that the electron density at these BCPs is low (Table 3), in the range commonly found for dispersion interactions, and considerably lower than was found previously for the stabilising H…H interactions identified for congested molecules.[45]

The C4 hydrogen atoms of the benzimidazolylidene rings participate in H···H bonding interactions with N-substituent hydrogen atoms in **N4b$^+$**, **N4b^0** and **N5b$^+$** (see Figure 2 for molecular graph of latter complex). These bond paths are shorter than $vdW_{H\cdots H}$, especially in the t-Bu-bearing **N5b$^+$**, and the electron densities at the BCPs are correspondingly higher.

In **N5b^0**, which has a different orientation of its t-Bu substituents, where two of the CH_3 groups are orientated forward as compared to only one in the two cationic species, C···H bonding interactions are observed in the same region. The C···H interatomic distances are significantly shorter than $vdW_{H\cdots C}$ (2.9 Å), suggesting that the observed bonding interactions have more to do with the forced proximity of the involved atoms than with their C or H identity. Based on the observed deviations in Au–C bond length trends for these species, we conclude that these BPs are indicative of steric repulsion; it is possible that with less congestion at the metal centre, an unfavourable interaction with the C4 hydrogen could be avoided. In the n-Bu substituted species the flexibility of the N-substituents appears to prevent this kind of unfavourable interaction.

Several weak Au···H bond paths can be identified in the molecular graphs of the complexes bearing NHCs with larger alkyl fragments (Figure 2 (b) and (c)). The t-Bu substituted species exhibit the most Au···H interactions, with a total of eight Au···H BCPs, with interatomic separations of 2.5 Å and 2.8 Å (compare sum of vdW radii 2.8 Å), being identified in **N5$^+$**. The BCP ρ, $\nabla^2\rho$, and kinetic energy density at the BCPs of the Au…H interactions in these four t-Bu substituted species and **N4b^0** all fall within ranges determined for weaker Au…H hydrogen bonds[48–50] and agostic interactions.[51] Au(I) is formally d^{10}, and the complexes in this study are known to be delocalised lipophilic cations,[52] implying a relatively homogeneous molecular charge distribution. It is therefore difficult to tell if the Au···H interactions are representative of agostic interactions, where electrons from the C–H bond donate into a transition metal orbital,[53,53] or hydrogen bonding, where electron density on the metal is polarised towards the C–H bond.[50] Au···H bonding interactions are observed in all the n-Bu substituted species, but in contrast to those observed for the t-Bu species, the interatomic distances all exceed $vdW_{Au\cdots H}$ (2.86 Å) and the BCP ρ falls outside the range for hydrogen bond or agostic interactions (but still in the range for weakly stabilising dispersion interactions).[55] It is interesting to note that the shortest H···H contact is found for **N5$^+$**, perhaps as a side effect of establishing the short Au···H contacts.

2.3. Electrostatic Surface Potentials

The Electrostatic Surface Potential (ESP) can reveal how a molecule is likely to engage in weak interactions, and is also related to its solubility properties.[56] ESPs calculated for the cationic Au-NHC complexes are very similar in terms of their charge distribution (Table 4). Besides the **N1$^+$**/**N1b$^+$** outliers, there is little variation in the maximum, minimum, and average potential on the molecular surface. A general decrease in these parameters is, however, observed with increasing volume, although the lowest values are obtained for **N5$^+$**/**N5b$^+$**. For the **Nxb$^+$** complexes, the maximum ESP tends to decrease more slowly with volume than the minimum, resulting in more variation across the molecular surface. The regions of charge accumulation and depletion can easily be discerned in ESP maps of the complexes. The ESP maps of **N1$^+$** and **N1b$^+$**, **N2b$^+$** and **N4$^+$** appear in Figure 3. The colour scale has been chosen according to the maximum and minimum charge areas of **N1b$^+$**, which has the largest ESP spread among the three complexes. The most positive areas (indicated in blue) on the isosurfaces of both **N1$^+$** and **N1b$^+$** occur close to the N-substituent, which corresponds to H atoms for these complexes. The areas of relative charge accumulation on these species (both isosurfaces are entirely positive) are quite different, however. The least positive area on **N1$^+$** is found in proximity to the aromatic carbons of the NHC rings, while in **N1b$^+$** much more electron density is concentrated above and below the benzene ring, as evidenced by the red colour on the isosurface. When the N-substituent H atoms are replaced by alkyl fragments (e.g. **N2b$^+$** and **N4$^+$**, Figure 3 (c) and (d)), a much more homogeneous charge distribution is observed, with the benzimidazolylidene-

Table 4. Electrostatic Surface Potential values and volumes of cationic complexes.

	Maximum (kcal mol^{-1})	Minimum	Average	Volume (bohr^3)
N1$^+$	118	62	83	1332
N1b$^+$	115	46	69	2114
N2$^+$	86	58	74	1938
N2b$^+$	77	43	65	2715
N3$^+$	86	56	69	2570
N3b$^+$	79	42	63	3344
N4$^+$	83	53	64	3163
N4b$^+$	75	41	60	3904
N5$^+$	79	52	62	3640
N5b$^+$	73	39	59	4375
N6$^+$	83	43	61	3791
N6b$^+$	76	40	57	4571

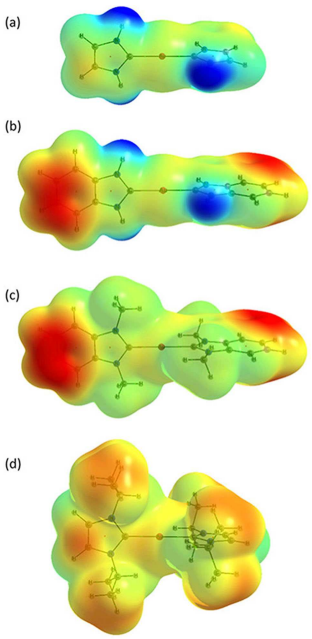

Figure 3. ESP maps of (a) **N1**$^+$, (b) **N1b**$^+$, (c) **N2b**$^+$ and d) **N4**$^+$. Red = 46 kcal/mol, blue = 115 kcal/mol.

containing complexes exhibiting lower maximum and minimum ESP values (Table 4). The ESP around Au in these complexes is close to the molecular surface average. The above observations are consistent with the results of a prior theoretical study and the reputation of these complexes as nonpolar.[4]

The neutral complexes show much greater variation in ESP over the entire molecular surface (Table 5), but the charge distribution across the NHC ligand is again very homogenous. Interestingly, the Au isosurface average ESP is slightly negative for these complexes, demonstrating the electronegativity of Au. The Cl atom exhibits the most negative ESP, while the NHC ligands appear mostly positive. We have previously shown that a concentration of electron density, which is often, but not always, associated with a slight negative charge on the gold allows the Au(I) centre to behave as a Lewis base and hence act as a hydrogen-bond acceptor.[48–50] The slightly negative ESP values for the Au thus suggest that the Au···H interactions identified for the **N4b**^{0} and the t-Bu substituted species in the AIM analysis above are indeed hydrogen bonds, rather than agostic interactions.

Table 5. Electrostatic Surface Potential values and volumes of neutral complexes.

	Maximum (kcal mol^{-1})	Minimum	Average	Volume (bohr^3)
N1^0	61	−42	3	1038
N1b^0	60	−41	4	1429
N2^0	40	−43	3	1340
N2b^0	33	−41	3	1729
N3^0	39	−43	2	1652
N3b^0	33	−41	3	2040
N4	39	−44	3	1954
N4b^0	31	−42	3	2325
N5^0	35	−43	2	2200
N5b^0	30	−42	2	2558
N6^0	31	−42	3	2266
N6b^0	31	−42	3	2656

2.4. Bond Dissociation Energies

Bond dissociation energies (BDEs) were calculated for NHC dissociation from the cationic and neutral complexes, see Figure 4 and Table S1 in the ESI. The cationic complexes display higher BDEs than the neutral complexes, as expected based on the higher stability of the neutral Au–Cl over the cationic Au-NHC fragment. In general, an upward trend in BDEs is observed as the size of the N-substituents is increased, with the t-Bu-substituted species being clear outliers. Significantly lower BDEs are observed for the t-Bu substituted species than for those bearing less sterically demanding N-substituents, and while the other imidazolylidene/benzimidazolylidene pairs differ little in terms of their BDEs, **N5b**$^+$ and **N5b**^{0} have BDEs ~10 kcal mol^{-1} lower than their imidazolylidene counterparts. This is likely related to steric repulsion, based on the long Au–C bond lengths noted earlier and what appear to be repulsive H···H interactions as discussed for the AIM analysis (*vide supra*). In the cationic species, the gap between imidazolylidene and benzimidazolylidene BDEs is slightly larger than in the neutral species, where the energy difference can almost be said to be insignificant. This is interesting considering that benzimidazolylidene ligands are considered to be less electron donating than imidazolylidene ligands, but here our results indicate that the

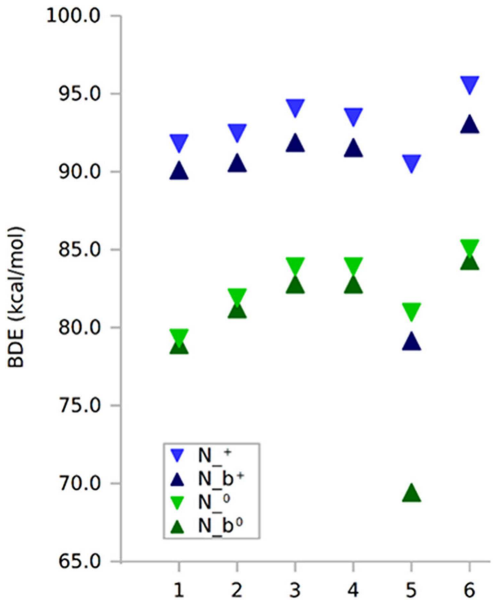

Figure 4. Bond dissociation electronic energies of cationic and neutral complexes, plotted in increasing order of molecular volume.

M-NHC bond strength may depend on the other ligands attached to the coordination complex.

2.5. Energy Decomposition Analysis

To gain greater insight into the BDEs, we performed Energy Decomposition Analysis (EDA) for the same bond dissociations described above. The results are shown in Figure 5 (numerical

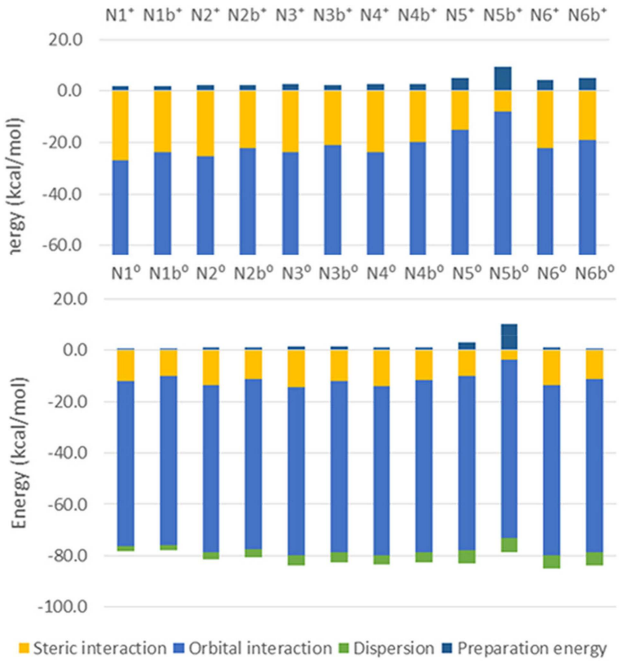

Figure 5. Energy decomposition of Au-NHC bonds in the (a) cationic complexes and (b) neutral complexes.

data may be found in Table S2 in the ESI), along with the preparation energy (energy required to deform the fragments from their isolated equilibrium structure to that observed in the complexes). The electrostatic and Pauli repulsion terms are the largest components of the energy (see Table S2 in the ESI), with the stabilising electrostatic term being marginally larger than the repulsive Pauli term so that grouping these terms together leads to a stabilising term that is reported as the steric term.[57] For the cationic species, as the volume of the N-substituent increases both the electrostatic and Pauli terms increase slightly but to different extents, such that the steric stabilisation decreases overall. However, the t-Bu species, **N5**$^+$ and **N5b**$^+$, have lower than expected Coulomb attraction and higher than expected Pauli repulsion given the observed trends, leading to steric terms that are much less stabilising than for the other species. The stabilising orbital term also increases with increasing volume of the N-substituent, but is a few kcal mol^{-1} higher in the t-Bu-substituted species, **N5**$^+$ and **N5b**$^+$. As expected, the stabilisation provided by dispersion interactions shows a general increase with the N-substituent volume.

Clear trends cannot be discerned in the individual energy terms of the neutral complex bond dissociations (except for a more stabilising dispersion interaction with increasing volume), but the total bond energy increases with increasing N-substituent size. For the t-Bu substituted species, both higher preparation energies as well as less stabilising steric terms as a result of smaller Coulombic terms are observed in both the cationic and neutral complexes, and this is more pronounced in the benzimidazolylidene species. Since this is observed in both the cationic and neutral species, this must be related to steric interactions between the ligands and the metal centre, as opposed to such interactions between opposing ligands.

2.6. Free Energy of Hydration

The free energies of hydration (ΔG_{hyd}) for the Au complexes were calculated using the COSMO-RS continuum solvation model. The results are shown in Tables 6 and 7.

Table 6. Free energies of hydration for cationic Au complexes.

	ΔG_{hyd} (kcal mol^{-1})		ΔG_{hyd} (kcal mol^{-1})
N1$^+$	−52.4	N1b$^+$	−49.6
N2$^+$	−35.2	N2b$^+$	−32.7
N3$^+$	−33.4	N3b$^+$	−31.0
N4$^+$	−30.4	N4b$^+$	−28.9
N5$^+$	−29.2	N5b$^+$	−28.1
N6$^+$	−30.7	N6b$^+$	−27.9

Table 7. Free energies of hydration of neutral Au complexes.

	ΔG_{hyd} (kcal mol^{-1})		ΔG_{hyd} (kcal mol^{-1})
N1^0	−18.6	N1b^0	−17.2
N2^0	−11.0	N2b^0	−9.4
N3^0	−10.1	N3b^0	−8.6
N4^0	−9.7	N4b^0	−8.2
N5^0	−8.7	N5b^0	−7.9
N6^0	−9.2	N6b^0	−7.5

The cationic Au complexes (Table 6) are greatly stabilised by the continuum solvent model (up to 52 kcal mol^{-1} in the case of **N1**$^+$), as expected for a charged species, with the stabilisation found for the **Nxb**$^+$ species typically a few kcal mol^{-1} lower than for the imidazolylidene analogues. Among the **Nxb**$^+$ complexes the most stabilising ΔG_{hyd} is found for **N1b**$^+$. The exceptional behaviour of **N1**$^+$ and **N1b**$^+$ is most likely a result of the H atom N-substituents being the sites of highest charge depletion in the coordination complexes studied here, particularly for the **Nxb**$^+$ species. The greater charge polarisation in **N1**$^+$ and **N1b**$^+$ (Figure 3) results in greater stabilisation upon solvation. In general, a decrease in the magnitude of ΔG_{solv} is seen as the size of the species increases, consistent with the decreased charge polarisation found in the larger complexes.

The neutral complexes exhibit more moderate ΔG_{hyd} values (Table 7), with the **N1^0** and **N1b^0** species again appearing as outliers.

2.7. Lipophilicity

The octanol-water partition coefficient was also calculated for the range of Au complexes using COSMO-RS. The results are shown in Tables 8 and 9, along with the average ESP and molecular volume calculated by the AIM approach. Experimental log P values are available for five of the cationic Au-NHC complexes.[16]

Table 8. Average ESP, volume, and log P of cationic Au complexes.

	ESP average (kcal mol^{-1})	Volume (bohr^3)	log P (calc)	log P (exp)
N1$^+$	83	1332	3.4	
N1b$^+$	69	2114	6.0	
N2$^+$	74	1938	4.8	−1.09
N2b$^+$	65	2715	7.0	
N3$^+$	69	2570	6.3	−0.8
N3b$^+$	63	3344	8.4	
N4$^+$	64	3163	9.0	
N4b$^+$	60	3904	10.3	
N5$^+$	62	3640	8.9	0.3
N5b$^+$	59	4375	10.6	
N6$^+$	61	3791	9.6	1.09
N6b$^+$	57	4571	11.6	

Table 9. Average ESP, volume, and log P of neutral Au complexes.

	ESP average (kcal mol^{-1})	Volume (bohr^3)	log P (calc)
N1^0	3	1038	0.9
N1b^0	4	1429	2.3
N2^0	3	1340	1.8
N2b^0	3	1729	3
N3^0	2	1652	2.8
N3b^0	3	2040	4
N4	3	1954	3.7
N4b^0	3	2325	4.9
N5^0	2	2200	4.2
N5b^0	2	2558	5.2
N6^0	3	2266	4.9
N6b^0	3	2656	6

It is immediately evident that the calculated log P values are grossly overestimated (Table 8), *i.e.* the continuum solvent model overestimates the affinity of the complexes for octanol relative to water. This is likely primarily due to the absence of the counterions, Cl^- and Br^-, in the calculation. In the physical experiment these anions are likely to have a low affinity for the octanol layer and a high affinity for the water layer (ΔG_{hyd} for Cl^- was calculated to be 70 kcal mol^{-1}). Besides the neglect of thisstabilisation, the potential difference established at the octanol-water interface by the differential partitioning of the Au complexes and counterions in the two solvent layers is also not accounted for in the calculation. This potential difference will limit the partitioning of the Au complexes into the octanol layer. Estimated solvent model parameters were used for Au (as described in the Computational Details section below), which may have an effect, but this is not easily predictable. Assuming that any error originating from the estimated parameters will affect the individual Au complex log P values to the same extent, the trends in the data can still provide meaningful insight. For the cationic complexes (Table 8), log P is observed to increase as the average ESP decreases and the molecular volume increases. Plotting log P as a function of the average ESP (Figure 6) and the volume (Figure 7) reveals linear trends with coefficients of determination close to unity. This is the case for both the calculated and experimental log P values. Despite the large nominal differences in calculated and experimental log P values, prediction of the relative lipophilicity of such delocalised lipophilic cations may be possible by using this approach. The neutral complexes also display log P values correlated with molecular volume (Figure 7), however there is no apparent relationship with the ESP values.

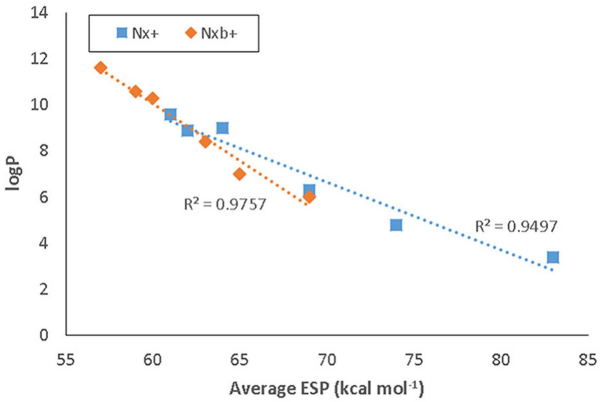

Figure 6. Log P relation to ESP average for cationic complexes.

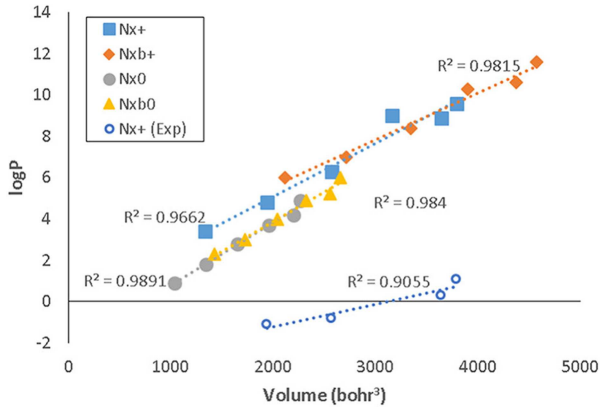

Figure 7. Log P relation to volume for all complexes.

3. Discussion

Through analysis of the electron density topology of a series of cationic and neutral Au(I)-NHC compounds we have shown that numerous bonding interactions, as defined by Bader, take place in these complexes, between ligands on opposite sides of the metal centre, among atoms of the ligands themselves, and between the ligands and metal centre. While the presence of these bond paths shows that it is energetically beneficial to accumulate electron density between the involved atoms, the effect on the system as a whole is more difficult to gauge, as has recently been pointed out by Wick and Clark.[37] The BCP properties would seem to indicate stabilising dispersion interactions, and this is in agreement with the EDA results, where more dispersion stabilisation is observed for the larger species (which also feature more bonding interactions). However, the structural aberrations, high preparation energies, and the increase of Pauli repulsion relative to Coulombic attraction observed in the t-Bu species suggest steric strain. Furthermore, in considering the EDA terms, ESPs and AIM results together the largest differences between the **N5b$^+$** and **N5b^0** species relative to **N5$^+$** and **N5^0** are the presence of the interactions between C4 hydrogen atoms of the benzimidazolylidene rings with N-substituent atoms. For the cationic complexes the Coulombic, Pauli, orbital and dispersion terms of the EDA for the imidazolylidene and benzimidazolylidene species differ by less than 4 kcal mol^{-1}, with the exception of the Coulombic term of **N5b$^+$**, which is almost 10 kcal mol^{-1} less stable than **N5$^+$**. We therefore credit the C4–H···H interaction with the destabilisation of the Au–C bond, which in turn leads to lower BDEs for these species. This has important implications for the use of such complexes in biological applications.

In the species bearing flexible n-Bu substituents, which are slightly larger than the t-Bu substituents, the highest number of bonding interactions between ligand atoms are observed, but these complexes do not appear to be sterically strained. Therefore, although going from an imidazolylidene to a benzimidazolylidene ligand is thought to mainly affect the electronic properties of the ligand, we conclude that it may lead to the introduction of significant steric strain in a metal complex, depending on the moiety present at the N-substituent position. Functionalisation at the C4 position could be an effective strategy to introduce steric strain at the metal centre even when the N-substituents are relatively small. On the other hand, this implies that unwanted steric repulsion may be introduced inadvertently when the heterocycle is modified to alter the electronic properties of a ligand.

4. Conclusions

The results shown here highlight the delicate balance between steric and electronic effects that play a role in the properties of Au-NHC complexes as possible prodrugs, where, in addition to low BDEs and high lipophilicities, it appears that intermolecular interactions present could also affect their mechanism of action. All the analyses undertaken show that there are significant differences between the imidazolylidene and benzimidazolylidene NHCs; the variation in ESPs, BDEs and EDA for these species confirm that electronic effects play a role, whereas the AIM highlights the steric differences. Similarly, although it has been suggested that the N-substituents have little effect on the electronic properties[14] the calculated differences in BDEs, ESPs and EDA suggest that this is also not entirely true. Furthermore, both volume, which is typically seen as being related to sterics, and ESP influence the lipophilicities, at least for the cationic complexes. This is probably related to the more homogenous charge distributions exhibited by the larger complexes, but also the volume-surface area connection, as the COSMO-RS model accounts for vdW-type interactions between solute and solvent. We have shown that although our calculated log P values differ significantly from experimental values, both show a linear relation to the molecular volume which may be useful in predicting the lipophilicity of related compounds.

It has previously been shown that at 1 μM concentration the n-Bu complex, N6$^+$, induces greater mitochondrial swelling than the t-Bu complex, N5$^+$, which was also found to correspond with the relative lipophilicities of the two complexes,[16] as confirmed by the calculations described here. However, at 10 μM the t-Bu has greater mitochondrial activity, which appears to correlate better with the relative order of the BDE results, suggesting that the influences of both the BDE and lipophilicity, which work in opposite directions relative to the size of the molecule, are important. A further factor may be the presence of the intramolecular interactions within the complex, where competition between the intramolecular interactions and intermolecular interactions with the TrxR enzyme active site may influence the mechanism of action of the prodrug. The next step of the study is therefore to study the interaction of the complexes with the TrxR enzyme active site in order to investigate this latter possibility. In particular, since the strength of the Au-ligand bond may be important in determining how easily ligand exchange with the may occur, the BDEs suggest that complexes with benzimidazolylidene ligands may be better prodrugs as these NHC ligands could be replaced more easily, so this aspect will be further investigated.

Computational Details

Geometry Optimisation

Geometry optimisations were performed with the Gaussian 09 Revision D.01 computational chemistry software package,[58] using the PBE0 density functional[59] and the def2-TZVP basis set for all atoms,[60] with a relativistic effective core potential (ECP) for gold.[61] The basis set and ECP were obtained from the EMSL basis set exchange.[62,63] Grimme's D3 dispersion correction (original damping function) was applied in all optimisations.[64] PBE0 was chosen as it has been extensively benchmarked (particularly in combination with def2-TZP) and shows good performance in describing transition metal complex geometries, thermochemistry and dispersion interactions when combined with Grimme's dispersion correction.[65–68] Furthermore, the method produces results in good agreement with high level coupled cluster calculations for the description of complexes of Au(I) and Au(III) with unsaturated

hydrocarbons,[69] and has recently been used to study Au(I) NHC complexes with phosphane ligands.[70] Stationary points were characterised by harmonic vibrational analysis to ensure that they represent minima on the potential energy surface. Starting structures for geometry optimisation of the Au complexes were obtained from the Cambridge Structural Database (CSD),[22] omitting counter-ions and solvent molecules. For those complexes where a crystal structure was not available, an initial geometry was constructed using the bond lengths and angles of similar complexes. Additionally, we probed the conformational space by performing relaxed scans of the torsion angle between the opposing NHC rings, and varying the orientation of the N-substituents in the starting structures for geometry optimisation. Bond Dissociation Energies (BDEs) for the ligands dissociating from the coordination complex were calculated as the difference between the energy of the coordination complex and the sum of the energies of the ligand of interest and the remainder of the coordination complex in their relaxed state. Images were generated with the Chemcraft suite.[71]

Atoms in Molecules

Atoms in Molecules (AIM) calculations were performed and images of molecular graphs were generated using our in-house program, eDensity.[72,73] Wave function files were prepared using the ORCA computational chemistry program package,[74] calculations being performed at the same level of theory as the geometry optimisations. However, although good optimised geometries may be derived using ECPs, information on the core electrons of heavy atoms is lost. This leads to several problems when performing AIM analysis. Therefore an all electron scalar relativistic (SARC) basis set was used for Au,[75] with relativistic effects further described with the aid of the zeroth order regular approximation (ZORA).[76–78]

Electrostatic Potential

The AIMAll software package version 15.05.18[79] was used for the calculation of the electrostatic surface potential (ESP) at an electron density of 0.001 $e\,\mathrm{bohr}^{-1}$. In mapping the function onto the 0.001 $e\,\mathrm{bohr}^{-1}$ isosurface the range of the colour scale was chosen to convey the variation of the ESP across the molecular isosurface, with the same range used for all complexes to facilitate comparison between complexes.

Energy Decomposition Analysis

Energy decomposition analysis (EDA) calculations were performed using an adaptation of the Morokuma bond energy decomposition scheme[80–72] implemented in the Amsterdam Density Functional (ADF) program package.[83,84] The PBE0 functional was combined with the triple zeta all electron ZORA/TZP basis set[85] and Grimme's D3 dispersion correction.[64]

Free Energy of Hydration and Octanol/Water Partition Coefficient

The free energy of hydration and the octanol/water partition coefficient were calculated using the COSMO-RS continuum solvation model[86,87] as implemented in ADF. Optimised structures from gas phase G09 calculations were used without further optimisation in the continuum solvation environment. This was done due to time constraints and also because the parameterisation of the COSMO-RS model in ADF was performed on gas phase structures only. The COSMO-RS parameterisation within ADF was done using the Becke Perdew exchange correlation functional, with the ZORA approximation for relativistic effects and the TZP small core basis set. These same settings were used for all COSMO-RS calculations described in this work, with a TZ2P basis set for Au, as recommended for heavy atoms.

Default options were used as far as possible, but Se and Au were not included in the parameterisation and some quantities had to be estimated for these atoms, i.e. the solvent radii and the element specific dispersion constants. The radii of the spheres which surround the solute atoms within the continuum are parameterised values and not directly derived from fundamentals, nevertheless these radii correlate well with Bondi radii.[86,87,47] A comparison is shown in Table 1. The average of the ratios between the COSMO-RS and Bondi radii is ~1.16, but since the ratio for heavier atoms tends to be closer to 1.17, we opted to select this ratio for Au, multiplying its Bondi radius by this amount to arrive at the solvent radii used for COSMO-RS calculations (Table 10).

Table 10. COSMO-RS and Bondi radii.

Element	Radii (Å) COSMO-RS	Bondi	Ratio
H	1.30	1.20	1.08
C	2.00	1.70	1.18
N	1.83	1.55	1.18
O	1.72	1.52	1.13
F	1.72	1.47	1.17
P	2.13	1.80	1.18
S	2.16	1.80	1.20
Cl	2.05	1.75	1.17
Br	2.16	1.85	1.17
I	2.32	1.98	1.17
Au	1.94[a]	1.66	1.17[a]

[a]Values chosen for this study.

The dispersion constants are also fitted values, deriving mainly from the dispersion energy gain of the solute making the transition from the gas to the condensed phase. However, other free energy contributions related to molecular size may be involved as well, which is problematic for an approach in determining such a constant without parameterisation. Due to the lack of appropriate experimental data and the considerable computational expense of such an activity, we opted instead to estimate dispersion constants for Au from their atomic polarisabilities.[88] The atomic polarisabilities of the atoms included in the COSMO-RS parameterisation were plotted with their dispersion constants, presuming a linear relationship (Figure 8). The value for nitrogen is particularly low, as noted by Klamt,[89] and so it was not included. The coefficient of

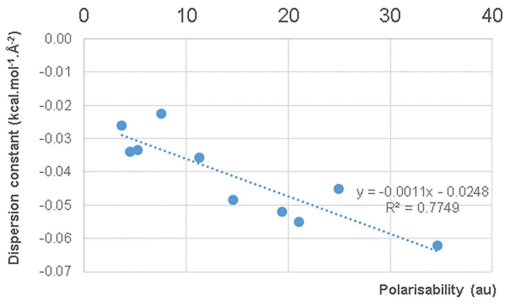

Figure 8. COSMO-RS dispersion constants as a function of atomic polarisability.

determination indicates a reasonable fit of the data. Inserting the polarisability of Au into the fit equation yields a dispersion constant of -0.0555 kcal.mol^{-1}Å^{-2}.

Acknowledgements

JD and CE thank the NRF for funding (JD: CSUR grant no. 91553; CE: CPRR grant no. 113331), while SdK thanks the Wilhelm Frank Trust for a scholarship. The Centre for High Performance Computing's Lengau cluster (http://www.chpc.ac.za/index.php/resources/lengau-cluster) and Stellenbosch University's Rhasatsha cluster (http://www.sun.ac.za/hpc) are thanked for computational resources. Opinions expressed and conclusions arrived at are those of the authors and are not necessarily to be attributed to the NRF.

Conflict of Interest

The authors declare no conflict of interest.

Keywords: computational chemistry · density functional calculations · gold complexes · intramolecular interactions · steric effects

[1] A. J. Arduengo, M. Kline, R. L. Harlow, *J. Am. Chem. Soc.* **1991**, *113*, 361–363.
[2] M. N. Hopkinson, C. Richter, M. Schedler, F. Glorius, *Nature* **2014**, *510*, 485–96.
[3] R. H. Crabtree, *J. Organomet. Chem.* **2005**, *690*, 5451–5457.
[4] D. J. Nelson, S. P. Nolan, *Chem. Soc. Rev.* **2013**, *42*, 6723–53.
[5] S. P. Nolan, Ed., *N-Heterocyclic Carbenes: Effective Tools for Organometallic Synthesis*, Wiley-VCH, Weinheim **2014**.
[6] F. Glorius, Ed., *N-heterocyclic Carbenes in Transition Metal Catalysis*, Springer, Berlin **2007**.
[7] L. Oehninger, R. Rubbiani, I. Ott, *Dalton Trans.* **2013**, *42*, 3269–3284.
[8] K. M. Hindi, M. J. Panzner, C. A. Tessier, C. L. Cannon, W. J. Youngs **2009**, 3859–3884.
[9] D. G. Gusev, *Organometallics* **2009**, *28*, 6458–6461.
[10] H. Clavier, A. Correa, L. Cavallo, E. C. Escudero-Adán, J. Benet-Buchholz, A. M. Z. Slawin, S. P. Nolan, *Eur. J. Inorg. Chem.* **2009**, 1767–1773.
[11] C. A. Urbina-Blanco, X. Bantreil, H. Clavier, A. M. Z. Slawin, S. P. Nolan, *Beilstein J. Org. Chem.* **2010**, *6*, 1120–1126.
[12] S. Díez-González, S. P. Nolan, *Coord. Chem. Rev.* **2007**, *251*, 874–883.
[13] S. Leuthäußer, D. Schwarz, H. Plenio, *Chem. Eur. J.* **2007**, *13*, 7195–7203.
[14] R. A. Kelly III, H. Clavier, S. Giudice, N. M. Scott, E. D. Stevens, J. Bordner, I. Samardjiev, C. D. Hoff, L. Cavallo, S. P. Nolan, *Organometallics* **2008**, *27*, 202–210.
[15] M. V Baker, P. J. Barnard, S. J. Berners-Price, S. K. Brayshaw, J. L. Hickey, B. W. Skelton, A. H. White, *J. Organomet. Chem.* **2005**, *690*, 5625–5635.
[16] M. V Baker, P. J. Barnard, S. J. Berners-Price, S. K. Brayshaw, J. L. Hickey, B. W. Skelton, A. H. White, *Dalton Trans.* **2006**, *6*, 3708–3715.
[17] R. Rubbiani, S. Can, I. Kitanovic, H. Alborzinia, M. Stefanopoulou, M. Kokoschka, S. Mönchgesang, W. S. Sheldrick, S. Wölfl, I. Ott, *J. Med. Chem.* **2011**, *54*, 8646–8657.
[18] R. Rubbiani, L. Salassa, A. De Almeida, A. Casini, I. Ott, *ChemMedChem.* **2014**, *9*, 1205–1210.
[19] A. Pratesi, C. Gabbiani, E. Michelucci, M. Ginanneschi, A. M. Papini, R. Rubbiani, I. Ott, L. Messori, *J. Inorg. Biochem.* **2014**, *136*, 161–9.
[20] D. Mustacich, G. Powis, *Biochem. J.* **2000**, *346*, 1–8.
[21] S. Urig, K. Becker, *Semin. Cancer Biol.* **2006**, *16*, 452–465.
[22] C. R. Groom, I. J. Bruno, M. P. Lightfoot, S. C. Ward, *Acta Crystallogr. Sect. B* **2016**, *72*, 171–179.
[23] P. C. Kunz, C. Wetzel, S. Kögel, M. U. Kassack, B. Spingler, *Dalton Trans.* **2011**, *40*, 35–37.
[24] Y. Chen, G. Cheng, K. Li, D. P. Shelar, W. Lu, C.-M. Che, *Chem. Sci.* **2014**, *5*, 1348–1353.
[25] T. J. Siciliano, M. C. Deblock, K. M. Hindi, S. Durmus, M. J. Panzner, C. A. Tessier, W. J. Youngs, *J. Organomet. Chem.* **2011**, *696*, 1066–1071.
[26] H. M. J. Wang, C. S. Vasam, T. Y. R. Tsai, S. Chen, A. H. H. Chang, I. J. B. Lin, *Organometallics* **2005**, *24*, 486–493.
[27] M. Rodríguez-Castillo, D. Laurencin, F. Tielens, A. van der Lee, S. Clément, Y. Guari, S. Richeter, *Dalton Trans.* **2014**, *43*, 5978.
[28] R. Jothibasu, H. V. Huynh, L. L. Koh, *J. Organomet. Chem.* **2008**, *693*, 374–380.
[29] H. Sivaram, J. Tan, H. V. Huynh, *Organometallics* **2012**, *31*, 5875–5883.
[30] B. Jacques, J. Kirsch, P. De Frémont, P. Braunstein, *Organometallics* **2012**, *31*, 4654–4657.
[31] H. M. J. Wang, C. Y. L. Chen, I. J. B. Lin, *Organometallics* **1999**, *18*, 1216–1223.
[32] X. Xu, S. H. Kim, X. Zhang, A. K. Das, H. Hirao, S. H. Hong, *Organometallics* **2013**, *32*, 164–171.
[33] L. Ray, V. Katiyar, S. Barman, M. J. Raihan, H. Nanavati, M. M. Shaikh, P. Ghosh, *J. Organomet. Chem.* **2007**, *692*, 4259–4269.
[34] M. C. Jahnke, J. Paley, F. Hupka, J. J. Weigand, F. E. Hahn, *Zeitschrift fur Naturforsch. - Sect. B J. Chem. Sci.* **2009**, *64*, 1458–1462.
[35] F. Mohr, *Gold Chemistry: Applications and Future Directions in the Life Sciences*, Wiley-VCH, Weinheim, Germany **2009**.
[36] R. F. W. Bader, *J. Phys. Chem. A* **1998**, *5639*, 7314–7323.
[37] C. R. Wick, T. Clark, *J. Mol. Model.* **2018**, *24*, 142.
[38] C. F. Matta, J. Hernández-Trujillo, T.-H. Tang, R. F. W. Bader, *Chem. Eur. J.* **2003**, *9*, 1940–1951.
[39] J. Poater, M. Solà, F. M. Bickelhaupt, *Chemistry* **2006**, *12*, 2889–95.
[40] R. F. W. Bader, *Chem. Eur. J.* **2006**, *12*, 2896–2901.
[41] J. Poater, M. Solà, F. M. Bickelhaupt, *Chemistry* **2006**, *12*, 2902–5.
[42] A. Martín Pendás, E. Francisco, M. A. Blanco, C. Gatti, *Chem. Eur. J.* **2007**, *13*, 9362–9371.
[43] R. F. W. Bader, *J. Phys. Chem. A* **2009**, *113*, 10391–10396.
[44] P. Dem'yanov, P. Polestshuk, *Chem. Eur. J.* **2012**, *18*, 4982–4993.
[45] J. Dillen, *Int. J. Quantum Chem.* **2013**, *113*, 2143–2153.
[46] C. Foroutan-Nejad, S. Shahbazian, R. Marek, *Chem. Eur. J.* **2014**, *20*, 10140–10152.
[47] A. Bondi, *J. Phys. Chem.* **1964**, *68*, 441–451.
[48] F. Groenewald, J. Dillen, H. G. Raubenheimer, C. Esterhuysen, *Angew. Chem. Int. Ed.* **2016**, *55*, 1694.
[49] F. Groenewald, J. Dillen, H. G. Raubenheimer, C. Esterhuysen, *Dalton Trans.* **2017**, 46, 4960.
[50] F. Groenewald, J. Dillen, H. G. Raubenheimer, C. Esterhuysen, *J. Mol. Model.* submitted.
[51] V. Tognetti, L. Joubert, R. Raucoules, T. De Bruin, C. Adamo, *J. Phys. Chem. A* **2012**, *116*, 5472–9.
[52] P. J. Barnard, S. J. Berners-Price, *Coord. Chem. Rev.* **2007**, *251*, 1889–1902.
[53] M. Brookhart, M. L. H. Green, G. Parkin, *Proc. Mont. Acad. Sci.* **2007**, *104*, 6908–6914.
[54] H. Schmidbaur, H. G. Raubenheimer, L. Dobrzańska, *Chem. Soc. Rev.* **2014**, *43*, 345–80.
[55] W. Nakanishi, S. Hayashi, K. Narahara, *J. Phys. Chem. A* **2008**, *112*, 13593–9.
[56] P. Politzer, P. Lane, J. Murray, T. Brinck, *J. Phys. Chem.* **1992**, *96*, 7938–7943.
[57] F. M. Bickelhaupt, E. J. Baerends, *Rev. Comput. Chem.* **2000**, *15*, 1–86.
[58] M. J. Frisch, G. W. Trucks, H. B. Schlegel, G. E. Scuseria, M. A. Robb, J. R. Cheeseman, G. Scalmani, V. Barone, G. Mennucci, A. Petersson, H. Nakatsuji, M. Caricato, X. Li, H. P. Hratchian, A. F. Izmaylov, J. Bloino, G. Zheng, J. L. Sonnenberg, M. Hada, M. Ehara, K. Toyota, R. Fukuda, J. Hasegawa, M. Ishida, T. Nakajima, Y. Honda, O. Kitao, H. Nakai, T. Vreven, J. A. M. Jr., J. E. Peralta, F. Ogliaro, M. Bearpark, J. J. Heyd, E. Brothers, K. N. Kudin, V. N. Staroverov, T. Keith, R. Kobayashi, J. Normand, K. Raghavachari, A. Rendell, J. C. Burant, S. S. Iyengar, J. Tomasi, M. Cossi, N. Rega, J. M. Millam, M. Klene, J. E. Knox, J. B. Cross, V. Bakken, C. Adamo, J. Jaramillo, R. Gomperts, R. E. Stratmann, O. Yazyev, A. J. Austin, R. Cammi, C. Pomelli, J. W. Ochterski, R. L. Martin, K. Morokuma, V. G. Zakrzewski, G. A. Voth, P. Salvador, J. J. Dannenberg, S. Dapprich, A. D. Daniels, O. Farkas, J. B. Foresman, J. V. Ortiz, J. Cioslowski, D. J. Fox, *Gaussian09*, **2013**.
[59] C. Adamo, V. Barone, *J. Chem. Phys.* **1999**, *110*, 6158.
[60] F. Weigend, R. Ahlrichs, *Phys. Chem. Chem. Phys.* **2005**, *7*, 3297–3305.
[61] D. Andrae, U. Häußermann, M. Dolg, H. Stoll, H. Preuß, *Theor. Chim. Acta* **1990**, *77*, 123–141.

[62] D. Feller, *J. Comput. Chem.* **1996**, *17*, 1571–1586.
[63] K. L. Schuchardt, B. T. Didier, T. Elsethagen, L. Sun, V. Gurumoorthi, J. Chase, J. Li, T. L. Windus, *J. Chem. Inf. Model.* **2007**, *47*, 1045–1052.
[64] S. Grimme, J. Antony, S. Ehrlich, H. Krieg, *J. Chem. Phys.* **2010**, *132*, 154104.
[65] L. Goerigk, S. Grimme, *Phys. Chem. Chem. Phys.* **2011**, *13*, 6670–6688.
[66] M. Bühl, C. Reimann, D. A. Pantazis, T. Bredow, F. Neese, *J. Chem. Theory Comput.* **2008**, *4*, 1449–1459.
[67] A. Karton, A. Tarnopolsky, J. F. Lamère, G. C. Schatz, J. M. L. Martin, *J. Phys. Chem. A* **2008**, *112*, 12868–12886.
[68] A. Hansen, C. Bannwarth, S. Grimme, P. Petrović, C. Werlé, J.-P. Djukic, *ChemistryOpen* **2014**, *3*, 177–189.
[69] R. Kang, H. Chen, S. Shaik, J. Yao, *J. Chem. Theory Comput.* **2011**, *7*, 4002–4011.
[70] R. Rubbiani, L. Salassa, A. De Almeida, A. Casini, I. Ott, *ChemMedChem* **2014**, *9*, 1205–1210.
[71] G. A. Zhurko, D. A. Zhurko, *ChemCraft* **2017**.
[72] J. Dillen, *J. Comput. Chem.* **2015**, *36*, 883–890.
[73] L.-M. Ferreira, A. Eaby, J. Dillen, *J. Comput. Chem.* **2017**, *38*, 2784–2790.
[74] F. Neese, *Wiley Interdiscip. Rev.: Comput. Mol. Sci.* **2012**, *2*, 73–78.
[75] D. A. Pantazis, X. Y. Chen, C. R. Landis, F. Neese, *J. Chem. Theory Comput.* **2008**, *4*, 908–919.
[76] E. van Lenthe, E. J. Baerends, J. G. Snijders, *J. Chem. Phys.* **1993**, *99*, 4597.
[77] E. van Lenthe, J. G. Snijders, E. J. Baerends, *J. Chem. Phys.* **1996**, *105*, 6505–6516.
[78] E. van Lenthe, R. van Leeuwen, E. J. Baerends, J. G. Snijders **1996**, *57*, 281–293.
[79] T. A. Keith, *AIMAll version 15.05.18*, TK Gristmill Software **2012**.
[80] K. Morokuma, *J. Chem. Phys.* **1971**, *55*, 1236–1244.
[81] K. Kitaura, K. Morokuma, *Int. J. Quantum Chem.* **1976**, *10*, 325–340.
[82] T. Ziegler, A. Rauk, *Theor. Chim. Acta* **1977**, *46*, 1–10.
[83] G. te Velde, F. M. Bickelhaupt, E. J. Baerends, C. Fonseca Guerra, S. J. A. van Gisbergen, J. G. Snijders, T. Ziegler, *J. Comput. Chem.* **2001**, *22*, 931–967.
[84] C. Fonseca Guerra, J. G. Snijders, G. Te Velde, E. J. Baerends, *Theor. Chem. Acc.* **1998**, *99*, 391–403.
[85] E. Van Lenthe, E. J. Baerends, *J. Comput. Chem.* **2003**, *24*, 1142–56.
[86] A. Klamt, V. Jonas, T. Bürger, J. C. W. Lohrenz, *J. Phys. Chem. A* **1998**, *102*, 5074–5085.
[87] A. Klamt, F. Eckert, *Fluid Phase Equilib.* **2000**, *172*, 43–72.
[88] P. Schwerdtfeger, Table of experimental and calculated static dipole polarizabilities for the electronic ground states of the neutral elements, http://ctcp.massey.ac.nz/dipole-polarizabilities (accessed 10 October 2015).
[89] A. Klamt, COSMO-RS: From Quantum Chemistry to Fluid Phase Thermodynamics and Drug Design, Elsevier, Amsterdam, The Netherlands **2005**.

Manuscript received: February 26, 2019